Geological Magazine

www.cambridge.org/geo

Geology and $^{40}Ar/^{39}Ar$ age of the Khopoli olivine gabbro intrusion, Konkan Plain, western Deccan Traps

Arunodaya Shekhar[1], Fred Jourdan[2], Ciro Cucciniello[3], Anmol Naik[1,4], Hetu Sheth[1] and B. Astha[1]

[1]Department of Earth Sciences, Indian Institute of Technology Bombay, Powai, Mumbai, India; [2]Western Australian Argon Isotope Facility, School of Earth and Planetary Science, JdL-CMS, SSTC and TiGeR, Curtin University, Perth, Australia; [3]Dipartimento di Scienze della Terra, dell'Ambiente e delle Risorse (DiSTAR), Università di Napoli Federico II, Complesso Universitario Monte Sant'Angelo, Via Cintia 21 (edificio L), Napoli, Italy and [4]School of Earth, Ocean and Atmospheric Sciences (SEOAS), Goa University, Taleigao, Goa, India

Original Article

Cite this article: Shekhar A, Jourdan F, Cucciniello C, Naik A, Sheth H, and Astha B. Geology and $^{40}Ar/^{39}Ar$ age of the Khopoli olivine gabbro intrusion, Konkan Plain, western Deccan Traps. *Geological Magazine* **161**(e12): 1–13. https://doi.org/10.1017/S0016756824000293

Received: 7 May 2024
Revised: 10 September 2024
Accepted: 12 September 2024

Keywords:
continental flood basalt; Deccan Traps; olivine gabbro; Khopoli; geological mapping; $^{40}Ar/^{39}Ar$ geochronology

Corresponding author:
Hetu Sheth; Email: hcsheth@iitb.ac.in

Abstract

The Khopoli intrusion is a small olivine gabbro intrusion exposed in the Konkan Plain, in the western part of the Deccan Traps continental flood basalt province. It intrudes lavas of the Neral and Thakurvadi formations, which belong to the lower part of the Western Ghats stratigraphic sequence and mainly comprise small-scale compound pāhoehoe flows and sheet lobes, respectively. Many of these lavas contain abundant cumulus olivine and clinopyroxene. The Khopoli intrusion is of considerable interest because its olivine gabbros are among the most magnesian Deccan rocks known, with bulk-rock MgO contents reaching 27 wt.%. Textural, mineralogical and geochemical features indicate that the olivine gabbros are olivine-pyroxene cumulates formed from an evolved tholeiitic basalt melt. Much of the original outcrop of the intrusion (mapped in 1980) is now lost owing to large-scale urban and industrial development. We have remapped the intrusion and obtained a $^{40}Ar/^{39}Ar$ age of 67.3 ± 1.5 Ma (2σ) on fresh intercumulus plagioclase grains separated from one of the olivine gabbros, which is consistent with the age of the host volcanic sequence. Measured true density values of 2.93 to 3.13 g/cm^3 for olivine gabbros of the Khopoli intrusion suggest possible shallow causes for at least some of the high gravity anomalies found in the Deccan Traps.

1. Introduction

The Late Cretaceous to Palaeocene-age Deccan Traps continental flood basalt (CFB) province in India (Fig. 1a) contains many plutonic complexes and dyke swarms (Deshmukh & Sehgal, 1988). A large number of these are exposed on the Konkan Plain, between the Western Ghats escarpment and the Arabian Sea (Fig. 1a,b), which forms part of the western Indian volcanic rifted margin (e.g., Yatheesh, 2020). The Konkan Plain intrusions show a great compositional diversity, varying from ultrabasic to silicic and from tholeiitic to strongly alkaline types (e.g., Sukheswala & Sethna, 1962; Godbole & Ray, 1996; Powar & Vadetwar 1995; Melluso *et al.* 2002; Dessai & Viegas, 2010; Naik *et al.* 2021). Of these, the Khopoli intrusion (Mulay & Peshwa, 1980, Fig. 2) is of considerable petrological interest in being one of the most magnesian rocks known in the Deccan province. The intrusion is composed of olivine gabbros with bulk-rock MgO contents reaching 27 wt.% (anhydrous basis), high Ni (733–883 ppm), Cr (1007–1432 ppm) and Co (109–125 ppm) contents, and very low incompatible element concentrations (Godbole & Ray, 1996; Melluso *et al.* 2010; Melluso & Sethna, 2011; Cucciniello *et al.* 2014). The olivine gabbros are composed of olivine, plagioclase, clinopyroxene, orthopyroxene, pigeonite and minor Fe-Ti oxides. Textural features and the chemistry of olivine and clinopyroxene indicate that the Khopoli olivine gabbros do not represent a high-MgO primitive liquid, but were formed as olivine-pyroxene cumulates from an evolved tholeiitic basalt melt (Mg# 49-58, where Mg# is 100 $Mg^{2+}/(Mg^{2+} + Fe^{2+})$, atomic). Isotopic ratios of Sr and Nd (initial $\varepsilon_{Nd}t = -9.0$ to -12.7 and $^{87}Sr/^{86}Sr = 0.7088$-0.7285) indicate compositional heterogeneity, and suggest that the basaltic melt from which the olivine gabbro cumulates formed had experienced variable degrees of contamination by ancient granitic basement crust (Cucciniello *et al.* 2014).

Despite the detailed information now available on the petrography, mineral and whole-rock geochemistry and petrogenesis of the Khopoli olivine gabbro intrusion (Melluso *et al.* 2010; Melluso & Sethna, 2011; Cucciniello *et al.* 2014), the shape and field relationships of the intrusion remain unclear. Mulay & Peshwa (1980) first mapped the Khopoli intrusion as three aligned elliptical outcrops separated and surrounded by the Deccan lava flows. Since their mapping, the area has undergone large-scale urban and industrial development, with much of the original outcrop area of the intrusion now covered. No age determinations on the intrusion

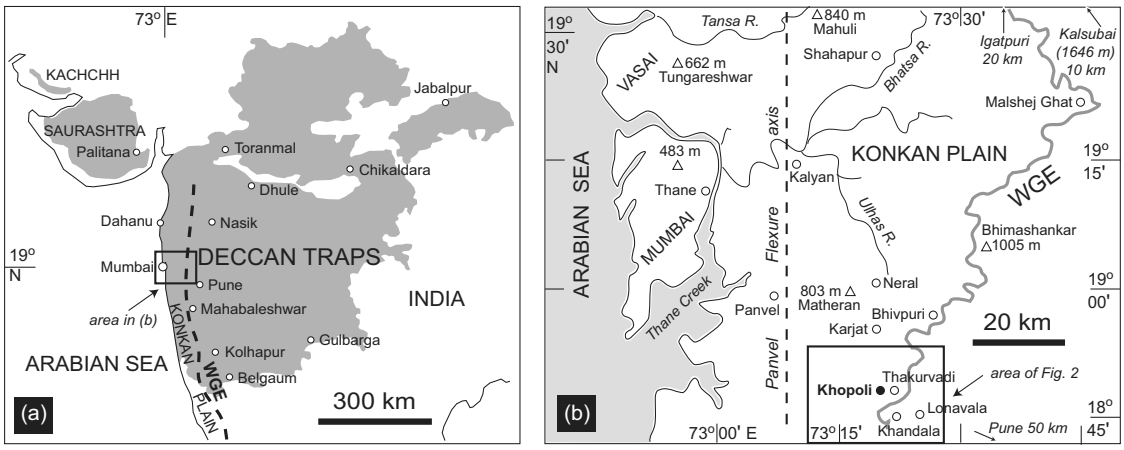

Figure 1. (a) Sketch-map of western-central India showing the Deccan Traps continental flood basalt province (grey), and some important localities within the province. WGE is the Western Ghats escarpment. (b) Map of part of the Konkan Plain, showing the topographic features, the study area of Khopoli and other localities mentioned in the text. The entire area is covered by the Deccan Traps. The volcanic sequence is horizontal east of the Panvel flexure axis but shows gentle to significant westerly dips west of the axis. Elevations (triangles) are in metres above mean sea level and 'R.' refers to rivers.

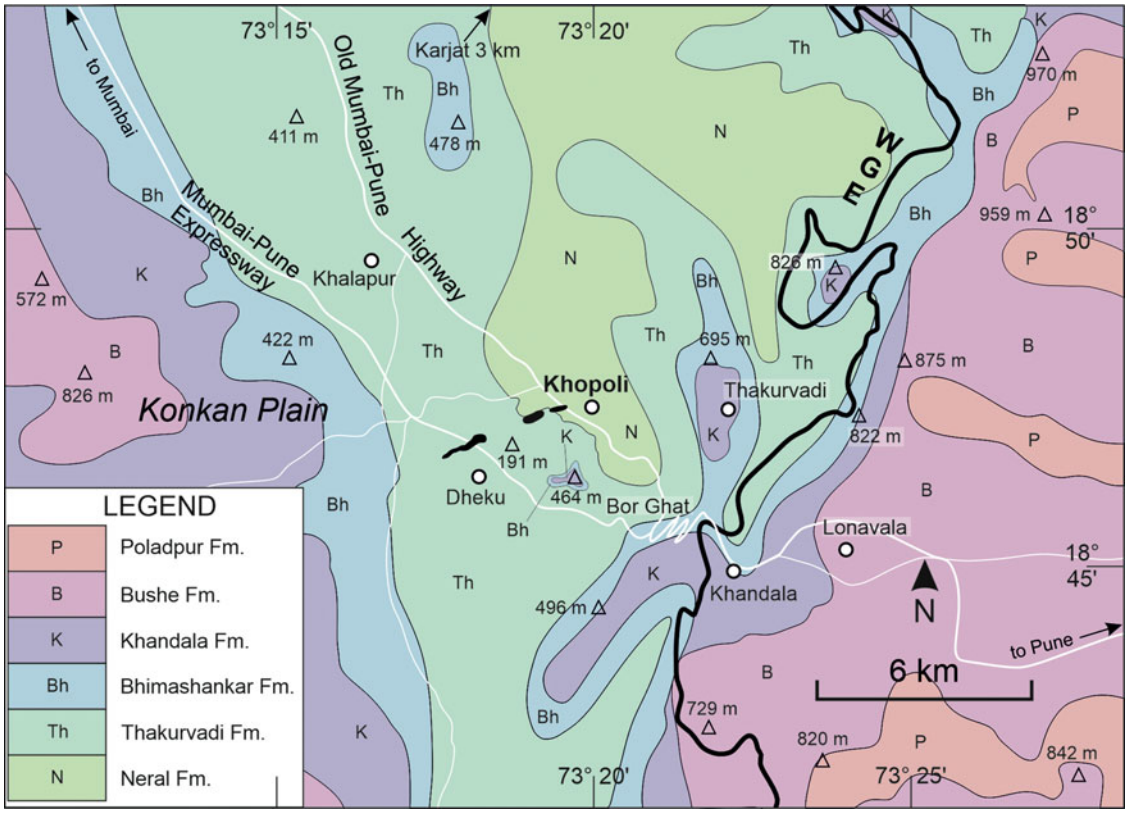

Figure 2. Geological map of the Khopoli area and surroundings, showing the Deccan lava stratigraphy (based on Beane, 1988; Subbarao & Hooper, 1988) superimposed on the major topographic features, especially the Western Ghats escarpment. The formations from Neral to Poladpur are progressively younger stratigraphically. Triangles are elevations in metres above mean sea level. The Khopoli olivine gabbro intrusion is shown as three black outcrops near the map centre. White lines are major roads and highways.

are available, and it is not known whether it formed contemporaneously with the host volcanic sequence (as suggested by Cucciniello *et al.* 2014 based on their geochemical similarities) or is considerably younger. We have therefore remapped and resampled the intrusion, and this contribution presents our field observations related to the geological context of the intrusion, its mineral and whole-rock geochemistry, its emplacement age determined with the $^{40}Ar/^{39}Ar$ dating technique, and true density measurements on the rocks of the intrusion. We use these varied datasets to discuss why the Khopoli intrusion is important not only for understanding the petrological evolution (specifically, cumulus processes) but also for geophysical observations in CFB provinces.

https://doi.org/10.1017/S0016756824000293 Published online by Cambridge University Press

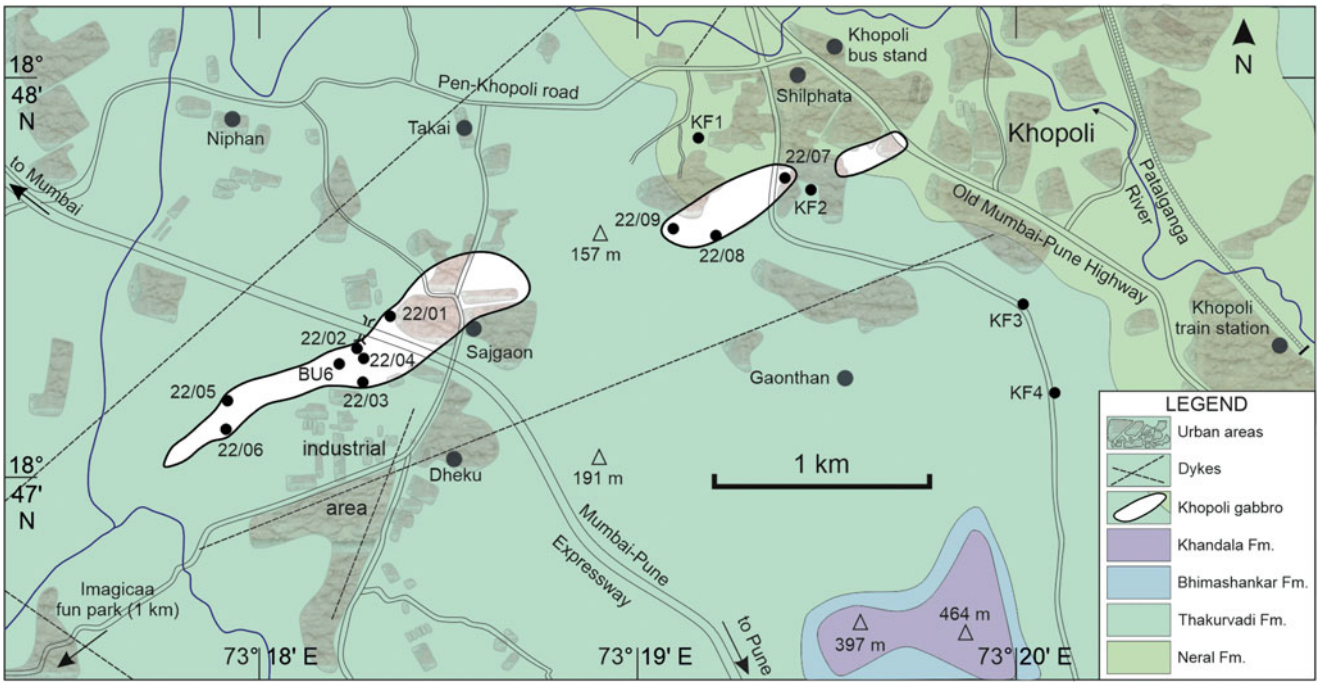

Figure 3. Geological map of the Khopoli intrusion (in white), based on Mulay & Peshwa (1980) and field mapping in the present study. Triangles are hills and peaks, with elevations reported in metres above mean sea level. The map also shows the urban developments (residential, commercial and industrial areas) that now cover the region, and major roads and highways (double lines). The outcrop areas of the Neral and Thakurvadi formations have been taken from Subbarao and Hooper (1988), but because their map is a much smaller-scale map, the boundary between the two formations has been suitably adjusted based on its elevation (e.g., Beane, 1988) and our field observations of outcrop features. Locations KF1 to KF4 are where we have made field observations of the lava flows, and these have the following geographic coordinates and elevations above mean sea level: KF1 (18° 47′ 50.6″ N, 73° 19′ 09.0″ E, 55 m), KF2 (18° 47′ 43.2″ N, 73° 19′ 27.5″ E, 94 m), KF3 (18° 47′ 25.6″ N, 73° 20′ 01.0″ E, 131 m), KF4 (18° 47′ 12.8″ N, 73° 20′ 05.7″ E, 162 m). Uncertainties in the coordinates and the elevations are ± 3 m. Locations KP22/01 to KP22/09 and BU6 (coordinates and elevations in Table 2) are where we have resampled the olivine gabbros; the prefix KP has not been shown in the map to avoid cluttering.

2. Field geology

2. a. Regional geological background

The Khopoli intrusion is exposed near the eastern edge of the Konkan Plain, at the base of the Western Ghats escarpment (Figs. 2, 3, 4a). It forms the lowermost elevations (~50–80 m above mean sea level) of the Bor Ghat section between the industrial town of Khopoli (61 m) and the hill resort of Khandala (624 m, on the escarpment) (Fig. 2). Geochemical stratigraphic mapping of this region (Subbarao and Hooper 1988 and references therein, Table 1) shows that the essentially horizontal host lava flows of the Khopoli intrusion belong to the Neral and Thakurvadi formations (Figs. 2, 3). The Neral Formation reaches its maximum thickness of 145 m near Bhivpuri (Fig. 1b) and thins to 80-100 m in the Neral and Bor Ghat areas (Beane *et al.* 1986). The Thakurvadi Formation has a maximum thickness of ~650 m, though it is ~210 m thick near Bor Ghat (Beane *et al.* 1986). The Neral and Thakurvadi Formations contain lava flows of evolved tholeiites, and also many lava flows of ankaramite, picritic basalt and picrite, with MgO contents reaching 25 wt.% in extreme cases (Mishra, 1971; Beane *et al.* 1986; Beane, 1988). These lava flows are enriched in cumulus olivine and clinopyroxene and do not represent primitive picritic liquids (Beane & Hooper, 1988; Khadri *et al.* 1988; Sethna & Sethna, 1990). The Thakurvadi Formation and the overlying Bhimashankar Formation constitute considerable thicknesses of some significant mountains on the Konkan Plain (e.g., Matheran, 803 m; Mahuli, 840 m, Fig. 1b), and much of the Western Ghats escarpment face (Figs. 2, 4a).

2. b. Field observations: lava flows

Lava flows exposed around the Khopoli intrusion are all pāhoehoe, and show a range of outcrop features (Fig. 4b-e). Karmarkar (1978) classified lava flows of the Bor Ghat section into tabular compact flows (thick and laterally extensive), tabular amygdaloidal flows (thinner and less extensive), thin, irregular amygdaloidal flows, and thick, irregular amygdaloidal flows. The former two categories are what are now called sheet lobes, whereas the latter two categories are compound flows (Sheth, 2018 and references therein). Karmarkar (1978) interpreted the tabular flows as large-volume flows produced by classical fissure eruptions and the compound flows as small-volume flows erupted from local, central-type vents.

Using modern terminology, we note that the lava flows of the Neral Formation form small-scale compound pāhoehoe lava flows, with numerous metre-scale or smaller flow units (lobes and toes, location KF1, Figs. 3, 4b-d). These flows show very well-developed internal structures such as sinuous lava feeder tubes (Fig. 4b), lava breakouts with ropy surfaces (Fig. 4b,c) and low tumuli with inflation clefts (Fig. 4d). In contrast, the lava flows of the overlying Thakurvadi Formation (e.g., locations KF3 and KF4, Fig. 3) are sheet lobes, tens of metres thick and laterally traceable for many kilometres (e.g., locations KF3 and KF4, Fig. 4e). These are much less weathered than the compound flows, and show fractures and crudely developed cooling joint columns. A large, abandoned rock quarry in the suburban area of Khopoli Shilphata (location KF2, Fig. 3) exposes a sheet lobe tens of metres thick with large-scale spheroidal weathering throughout.

https://doi.org/10.1017/S0016756824000293 Published online by Cambridge University Press

Figure 4. (a) Panoramic view of the Western Ghats escarpment, looking approximately northeast from location KF3 marked in Fig. 3. Buildings in the foreground provide an approximate scale. (b-d) Outcrop features of small-scale compound pāhoehoe lava flows of the Neral Formation at location KF1, in the southwestern part of the township of Khopoli Shilphata. (e) A typical Thakurvadi sheet lobe exposed at location KF4 and traceable for many kilometres. Persons provide a scale.

2. c. Field observations: the Khopoli intrusion

Mulay & Peshwa (1980) first mapped the Khopoli intrusion using remote sensing imagery and fieldwork. They showed that the intrusion comprised three elliptical outcrops aligned in a NE-SW direction, with a total length of ~4 km, and separated and surrounded by the Deccan lava flows. Large-scale urban and industrial development has taken place in the area since their original mapping, resulting in much of the original area of the Khopoli intrusion being now covered (Fig. 3). We have sampled the intrusion in two of the three elliptical outcrops that are still partly accessible (Fig. 3). The outcrops form flat terrain, the olivine gabbros are uniformly coarse and massive and those forming the largest outcrop show polygonal surficial jointing resembling 'tortoise-shell weathering' (Ollier, 1984) (Fig. 5a-c).

The easternmost segment of the Khopoli intrusion and the contacts of the other two segments with the basaltic lava flows (Fig. 3) are nowhere currently exposed and have been taken from the map by Mulay & Peshwa (1980). Our new geological map of the intrusion (Fig. 3) closely matches theirs, with the modification that our sample locations KP22/08 and KP22/09 increase the outcrop area of the intrusion by a few per cent.

Mulay & Peshwa (1980) also mapped a few mafic dykes around the olivine gabbro intrusion, forming one set that trends ~NE-SW (thus subparallel to the intrusion) and another set trending ~NW-SE. These are shown in Fig. 3. The dykes are poorly exposed today.

3. Analytical methods

3. a. Petrography and mineral chemistry

Thin sections of the Khopoli olivine gabbros were prepared by standard techniques. Petrographic observations were made in plane-polarised and cross-polarised light using a Leica DM2500 petrological microscope, and photomicrographs were taken with a Leica DFC295 camera attached to the microscope.

Back-scattered electron images were obtained, elemental X-ray maps were made and quantitative chemical analyses were performed with a scanning electron microscope (JEOL JSM-5310) equipped with an energy-dispersive X-ray detector (Oxford Instruments). The microanalysis unit was equipped with an INCA X-act detector, INCA X-stream pulse processor, energy software (with XPP matrix correction scheme) and INCA mics for acquisition of digital images. These were operated at 15 kV

https://doi.org/10.1017/S0016756824000293 Published online by Cambridge University Press

Table 1. Stratigraphy of the Deccan flood basalts in the Western Ghats, with formation thicknesses, magnetic polarity and Sr isotopic values (at 66 Ma)

Group	Sub-group	Formation	Magnetic polarity	$^{87}Sr/^{86}Sr_{(66\ Ma)}$
Deccan Basalt	Wai	Desur* (~100 m)	N	0.7072–0.7080
		Panhala (> 175 m)	N	0.7046–0.7055
		Mahabaleshwar (280 m)	N	0.7040–0.7055
		Ambenali (500 m)	R	0.7038–0.7044
		Poladpur (375 m)	R	0.7053–0.7110
	Lonavala	Bushe (325 m)	R	0.7078–0.7200
		Khandala (140 m)	R	0.7071–0.7124
	Kalsubai	Bhimashankar (140 m)	R	0.7067–0.7076
		Thakurvadi (650 m)	R	0.7067–0.7112
		Neral (100 m)	R	0.7062–0.7104
		Jawhar-Igatpuri (> 700 m)	R	0.7085–0.7128

*Considered by many as a 'Unit' of the Panhala Formation itself. Table based on Subbarao and Hooper (1988), Peng *et al.* (1994), and references therein. N = Normal magnetic polarity, R = Reverse magnetic polarity.

Figure 5. Outcrop features of the Khopoli olivine gabbros forming the largest outcrop, at three of the sampled locations. (a) Typical rounded boulders and blocks just south of the underpass in the Mumbai-Pune Expressway. (b,c) Polygonal jointing (tortoise-shell weathering) in the surficial parts of the olivine gabbro blocks. People for scale.

primary beam voltage, 50-100 μA filament current, 20 mm working distance and 50 s net acquisition time. The following standards were used for calibration: diopside (Mg), wollastonite (Ca), anorthoclase (Al, Si), albite (Na), rutile (Ti), almandine (Fe), Cr_2O_3 (Cr), rhodonite (Mn), orthoclase (K), apatite (P), fluorite (F), barite (Ba), strontianite (Sr), Smithsonian orthophosphates (REE, Y), pure niobium (Nb), pure vanadium (V), zircon (Zr, Hf), Corning glass (Th and U), sphalerite (S) and sodium chloride (Cl). Evaluation of analytical accuracy was done by checking against the above standards, INTAV (International Focus Group on Tephrochronology and Volcanism) glass (Kuehn *et al.* 2011) and Durango Apatite (cf. Cucciniello *et al.* 2020, 2023). Reference values of international standards for the SEM-EDS (scanning electron microscopy - energy dispersive X-ray spectroscopy) analyses are reported in Supplementary Table S1, and the mineral compositions are reported in Supplementary Table S2.

3. b. Whole-rock geochemistry

The nine olivine gabbro samples collected in this study (Fig. 3) were cut into small chips (~1 cm) using a diamond saw, and these were broken into 5 mm-size chips using a stainless steel mortar and pestle. The chips were cleaned in an ultrasonic bath using distilled water, dried and ground to powders of < 75 μm grain size using a

https://doi.org/10.1017/S0016756824000293 Published online by Cambridge University Press

Retsch PM-100 planetary ball mill and stainless steel grinding balls. The sample powders were dried in an oven at 110 °C overnight to remove any adsorbed moisture (H_2O^-), after which weight loss on ignition (LOI) was determined by heating the powders at 950 °C in platinum crucibles. For major oxide analysis, 7 g of the dry sample powders were mixed with 1 g of methyl cellulose binder and made into pressed pellets using an Insmart XRF 40 hydraulic press operated at a maximum load of 20 tonnes. The major oxides were analysed using a Rigaku ZSX Primus IV sequential wavelength-dispersive XRF spectrometer (4 kW) in the Department of Earth Sciences, IIT Bombay. Rock standards from the U. S. Geological Survey (BHVO-2, BCR-2 and W-2a) and the Geological Survey of Japan (JB-1b, JGb-2) were used for calibrating the instrument, and the U. S. Geological Survey standard DNC-1 (Dolerite North Carolina) was analysed along with the samples for estimating the analytical accuracy. The major oxide and LOI values are presented in Table 2, and previously available analyses of the olivine gabbros are tabulated in Supplementary Table S3.

3. c. $^{40}Ar/^{39}Ar$ geochronology

$^{40}Ar/^{39}Ar$ dating was carried out on plagioclase separates (representing the intercumulus phase) from the olivine gabbro sample BU6 (Figs. 6a, 7a). Approximately 16 mg of clean plagioclase grains (150–250 μm grain size) were hand-picked under a binocular microscope (Supplementary Fig. S1). Grains were leached in dilute HF for 5 min and then thoroughly rinsed with distilled water in an ultrasonic bath. The sample was then loaded in a disk into an aluminium foil packet, placed in a quartz tube, with the flux monitor standard Fish Canyon sanidine (FCs, 28.294 ± 0.036 Ma, 1σ; Renne *et al.* 2010), and irradiated for 3 h in the Oregon State University nuclear reactor (USA) in the central position. The disks were Cd-shielded (to minimise undesirable nuclear interference reactions). The mean J-values computed from standard grains within the small pits yielded values of 0.010635 (± 0.05%). Mass discrimination was monitored regularly during the analysis using an automated air pipette, and provided mean values of 0.992665 (± 0.04%) per dalton (atomic mass unit) relative to an air ratio of 298.56 ± 0.31 (Lee *et al.* 2016). The correction factors for interfering isotopes (Renne *et al.* 2013) were $(^{39}Ar/^{37}Ar)_{Ca} = 7.6 \times 10^{-4}$ (± 1.2%), $(^{36}Ar/^{37}Ar)_{Ca} = 2.7 \times 10^{-4}$ (± 0.7%) and $(^{40}Ar/^{39}Ar)_{K} = 7.3 \times 10^{-4}$ (± 10%).

The $^{40}Ar/^{39}Ar$ analyses were performed at the Western Australian Argon Isotope Facility at Curtin University. Plagioclase crystals were step-heated using a continuous 100 W PhotonMachine© CO_2 (IR, 10.6 μm) laser fired on the crystals for 60 s for each step. Each of the standard crystals was fused in a single step. The gas was purified in an extra low-volume stainless steel extraction line of 240 cm^3 using one SAES AP10 and one GP50 getter. Argon isotopes were measured in static mode using a low-volume (600 cm^3) ARGUS VI mass spectrometer from Thermofisher© (Phillips & Matchan, 2013) set with a permanent resolution of ~200. Measurements were carried out in multi-collection mode using four faradays to measure masses 40 to 37 and a zero-background compact discrete dynode ion counter to measure mass 36. We measured the relative abundance of each mass simultaneously using 10 cycles of peak-hopping and 33 s of integration time for each mass. Detectors were calibrated to each other electronically and using Air shot beam signals.

The raw data were processed using the ArArCALC software (Koppers, 2002) and the ages were calculated using the decay constants recommended by Renne *et al.* (2011). Blanks were monitored every 3 to 4 steps. All parameters and relative abundance values are reported in Supplementary Table S4 and have been corrected for blank, mass discrimination and radioactive decay. Individual errors are given at the 1σ level in Supplementary Table S4. Following Jiang *et al.* (2021) and Merle *et al.* (2022), our criteria for the determination of plateaus are as follows: a plateau must include at least 70% of ^{39}Ar, and the plateau should be distributed over a minimum of three consecutive steps agreeing at the 95% confidence level and satisfying a probability of fit (P) of at least 0.05. Plateau ages are reported at the 2σ level and are calculated using the mean of all the plateau steps, each weighted by the inverse variance of their individual analytical error. Uncertainties include analytical and J-value errors. Errors with all sources of uncertainty are indicated (e.g., ± 0.16 Ma).

3. d. True density measurements

We measured the true density values of the Khopoli olivine gabbro samples, crushed to 5 mm-size chips, using 50 ml pycnometers and distilled water (density 0.997 g/cm^3 at 25 °C) (Supplementary Table S5). Unlike bulk density, which includes pore space volume (see van Keulen, 1973), true density is the density of a solid measured without including the volume of any pore spaces (both surface or internal, and connected or blind pores) during volume measurement. We measured the weight of each pycnometer that was successively empty, about half-full with the solid granular sample, half-full with the solid and the rest with water and full of water. The weights and volumes of the solid sample and water were calculated for the various situations, and the density of the solid was computed as the ratio of mass to volume, as shown in Supplementary Table S5.

4. Results

4. a. Petrography and mineral chemistry

The rock samples of this study, representing two preserved outcrops of the Khopoli intrusion, are petrographically very similar. The olivine gabbros are composed of 50–55% modal olivine, 20–25% plagioclase, 10–15% clinopyroxene, 5–10% low-Ca pyroxenes (orthopyroxene and pigeonite), < 5% Fe-Ti oxides and rare interstitial alkali feldspar. They show a well-developed poikilitic texture in which plagioclase encloses the ferromagnesian minerals (Fig. 6a-d). Olivine, the dominant phase, contains inclusions of Cr-rich spinel and is generally altered along fractures to serpentine or iddingsite. Several crystals are entirely serpentinised. The order of crystallization of the mineral phases is chromite, olivine, clinopyroxene, low-Ca pyroxene and plagioclase, with Fe-Ti oxides and accessory minerals occurring locally as cumulus phases (Cucciniello *et al.* 2014; see this paper for detailed mineral chemistry).

Mineral chemistry and element mapping of olivine gabbros show little chemical zonation (Fig. 7a,b). Cumulus olivine shows a narrow compositional range from Fo_{78} to Fo_{71} (where Fo = Mg/(Mg + Fe)*100). Cumulus clinopyroxene is augite and shows a small variation in Mg# (where Mg# = atomic Mg/(Mg + Fe_{tot}) *100) from 81 to 76. The clinopyroxene compositions plot within the field defined by clinopyroxenes in the Deccan tholeiitic basalts (the Thakurvadi, Khandala and Bushe formations) (Cucciniello *et al.* 2014). Cumulus orthopyroxene ($Wo_{5-3}En_{70-74}Fs_{25-21}$) and pigeonite are homogeneous. Intercumulus plagioclase ranges from labradorite (An_{68-53}) to andesine (An_{47-35}), with mostly normal

https://doi.org/10.1017/S0016756824000293 Published online by Cambridge University Press

Table 2. Major oxide and loss on ignition (LOI)data (in wt.%) for olivine gabbros from the Khopoli intrusion

Sample	KP22/01	KP22/02	KP22/03	KP22/04	KP22/05	KP22/06	KP22/07	KP22/08	KP22/09	DNC-1 Ref.	DNC-1 Meas.
Lat. (N)	18° 47’ 24.4”	18° 47’ 18.8”	18° 47’ 13.8”	18° 47’ 17.2”	18° 47’ 11.1”	18° 47’ 06.8”	18° 47’ 45.1”	18° 47’ 36.3”	18° 47’ 36.9”		
Long. (E)	73° 18’ 20.5”	73° 18’ 15.3”	73° 18’ 16.2”	73° 18’ 16.4”	73° 17’ 54.9”	73° 17’ 54.5”	73° 19’ 23.6”	73° 19’ 12.7”	73° 19’ 05.8”		
Elev. (m)	58	58	58	70	52	55	80	60	67		
SiO_2	46.35	44.84	44.28	44.06	44.78	44.51	45.05	44.79	45.46	47.15	46.95
TiO_2	1.30	0.85	0.84	0.70	0.76	0.81	0.75	0.81	0.75	0.48	0.46
Al_2O_3	7.30	4.85	4.60	4.05	4.45	4.30	4.95	4.67	4.64	18.34	17.65
Fe_2O_3(T)	15.70	15.61	16.18	16.77	16.51	16.21	15.22	17.16	16.00	9.97	9.98
MnO	0.21	0.22	0.22	0.23	0.22	0.22	0.21	0.23	0.22	0.15	0.15
MgO	20.18	21.03	21.39	22.84	22.93	22.15	20.79	23.25	21.82	10.13	10.11
CaO	6.73	6.37	6.21	5.65	5.76	5.94	7.65	5.17	6.68	11.49	11.60
Na_2O	1.41	0.67	0.62	0.70	0.57	0.62	0.71	0.73	0.65	1.89	1.85
K_2O	0.37	0.01	0.01	0.01	0.01	0.01	0.03	0.01	0.01	0.23	0.20
P_2O_5	0.19	0.11	0.10	0.10	0.10	0.10	0.11	0.12	0.09	0.07	0.09
LOI	0.78	5.19	4.78	4.81	5.65	4.51	4.78	3.50	5.41	–	–
Total	100.51	99.75	99.23	99.92	101.74	99.38	100.24	100.42	101.74	99.90	99.03
Mg#	75.0	75.9	75.6	76.1	76.4	76.1	76.1	76.0	76.1		

Notes: Latitudes, longitudes and elevations (in metres above mean sea level) of the samples of this study, with uncertainties of ± 3 m, are provided above. For sample BU6 these are 18° 47’ 17.1” N, 73° 18’ 12.7” E, ~60 m. Reference values for the USGS rock standard DNC-1 (Flanagan, 1984) and the measured values provide an idea about analytical accuracy. Mg Number (Mg#) = 100 $Mg^{2+}/(Mg^{2+} + Fe^{2+})$, atomic. Mg# values were calculated based on LOI-free adjusted data obtained with the SINCLAS program (Verma *et al.* 2002) and a Fe^{2+}/Fe^{3+} ratio following the iron division scheme of Middlemost (1989) offered by the program.

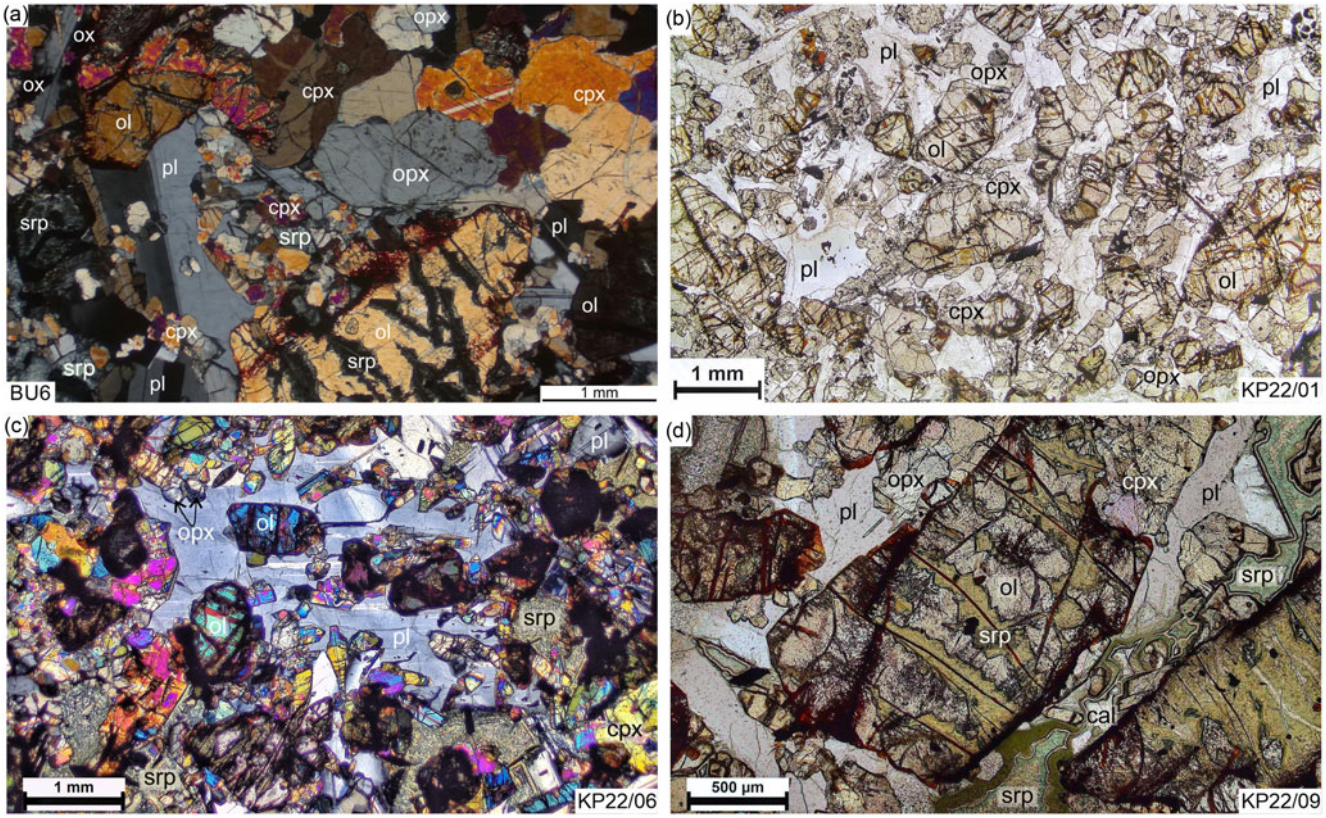

Figure 6. Photomicrographs of the Khopoli olivine gabbros. Abbreviations: ol, olivine; pl, plagioclase; cpx, clinopyroxene; opx, orthopyroxene; ox, opaque oxides; srp, serpentine; cal, calcite. (a) Sample BU6, crossed nicols. Large cumulus grains of olivine and clinopyroxene are observed, along with small grains of clinopyroxene and orthopyroxene which are often enclosed within large plagioclase grains (poikilitic texture). (b) Sample KP22/01, plane-polarised light. (c) Sample KP22/06, cross-polarised light. (d) Sample KP22/09, plane-polarised light.

compositional zoning (Supplementary Table S2; Cucciniello *et al.* 2014).

4. b. Whole-rock geochemistry

The LOI values for the olivine gabbros range from 0.78 wt.% (sample KP22/01) to 5.65 wt.% (sample KP22/05) (Table 2), whereas sample BU6 has a value of 6.00 wt.% (Supplementary Table S3). These mostly high LOI values indicate significant alteration of the rocks, consistent with the petrographic observations. Considered on an LOI-free basis, the Khopoli olivine gabbros have extremely high MgO (20.5–26.9 wt.%), with high Ni (733–883 ppm) and Cr (1432–1007 ppm), and low TiO_2 (0.7–0.8 wt.%), Al_2O_3 (< 6 wt.%) and CaO (4.9–6.8 wt.%) (Melluso *et al.* 2010; Cucciniello *et al.* 2014). Three samples analysed by Godbole & Ray (1996) have very similar concentrations of these elements (MgO 20.88–24.71 wt.%, Ni 609-708 ppm, Cr 1981–2391 ppm, TiO_2 0.95–0.97 wt.%, Al_2O_3 4.85–6.75 wt.%, CaO 6.47–7.26 wt.%); LOI data are not reported for two of these samples and the third has an LOI value of 3.66 wt.% (Supplementary Table S3). We note the following: (i) the dominance of olivine (mode 50–55%) in all samples, (ii) the absence of a correlation between MgO content and LOI in the samples of the present study (Table 2) and (iii) the high-MgO value of 20.18 wt.% for even the lowest-LOI sample (KP22/01, 0.78 wt.%). These observations suggest that, whereas alteration of these rocks is widespread and significant, their MgO contents are essentially a primary magmatic feature. These are among the most MgO-rich Deccan rocks. Mg numbers (Mg#) for the samples of the present study are high and remarkably uniform (75.0–76.4, Table 2), whereas previously analysed samples (Godbole & Ray, 1996; Melluso *et al.* 2010; Cucciniello *et al.* 2014) have higher Mg# values of 78–79 (Supplementary Table S3). Notably, SiO_2 contents recalculated LOI-free for the samples of the present study are all > 45 wt.% (the range being 46.9 to 48.1), and these olivine gabbros are thus basic, not ultrabasic, rocks.

4. c. $^{40}Ar/^{39}Ar$ geochronology

Fresh plagioclase separated from the sample BU6 gave a plateau age of 67.3 ± 1.5 Ma (MSWD = 0.10 and P = 1.0, 2σ, all uncertainties included), including 92% of the ^{39}Ar released (Fig. 8a). The inverse isochron age (67.7 ± 1.6 Ma, Fig. 8b) and the plateau age are identical, and the inverse isochron has an MSWD value of 0.01 and a $^{40}Ar/^{36}Ar$ intercept of 294.6 ± 6.9, again within error of the value of the atmospheric ratio. The low K/Ca ratios (0.0112 ± 0.0002) as calculated from $^{39}Ar/^{37}Ar$ (Fig. 8a) are consistent with the chemical compositions of the analysed phases as determined by energy-dispersive X-ray spectroscopy measurements (Supplementary Tables S2 and S4). The low MSWD and high P values for the plateau and inverse isochron indicate error overestimation or the presence of correlated errors. The high P and the high age uncertainty of > 2% result from the fact that there was very little material to analyse. We interpret the plateau age of 67.3 ± 1.5 Ma (2σ) obtained on the plagioclase separates as the best estimate of the time of emplacement and crystallization of the Khopoli intrusion.

https://doi.org/10.1017/S0016756824000293 Published online by Cambridge University Press

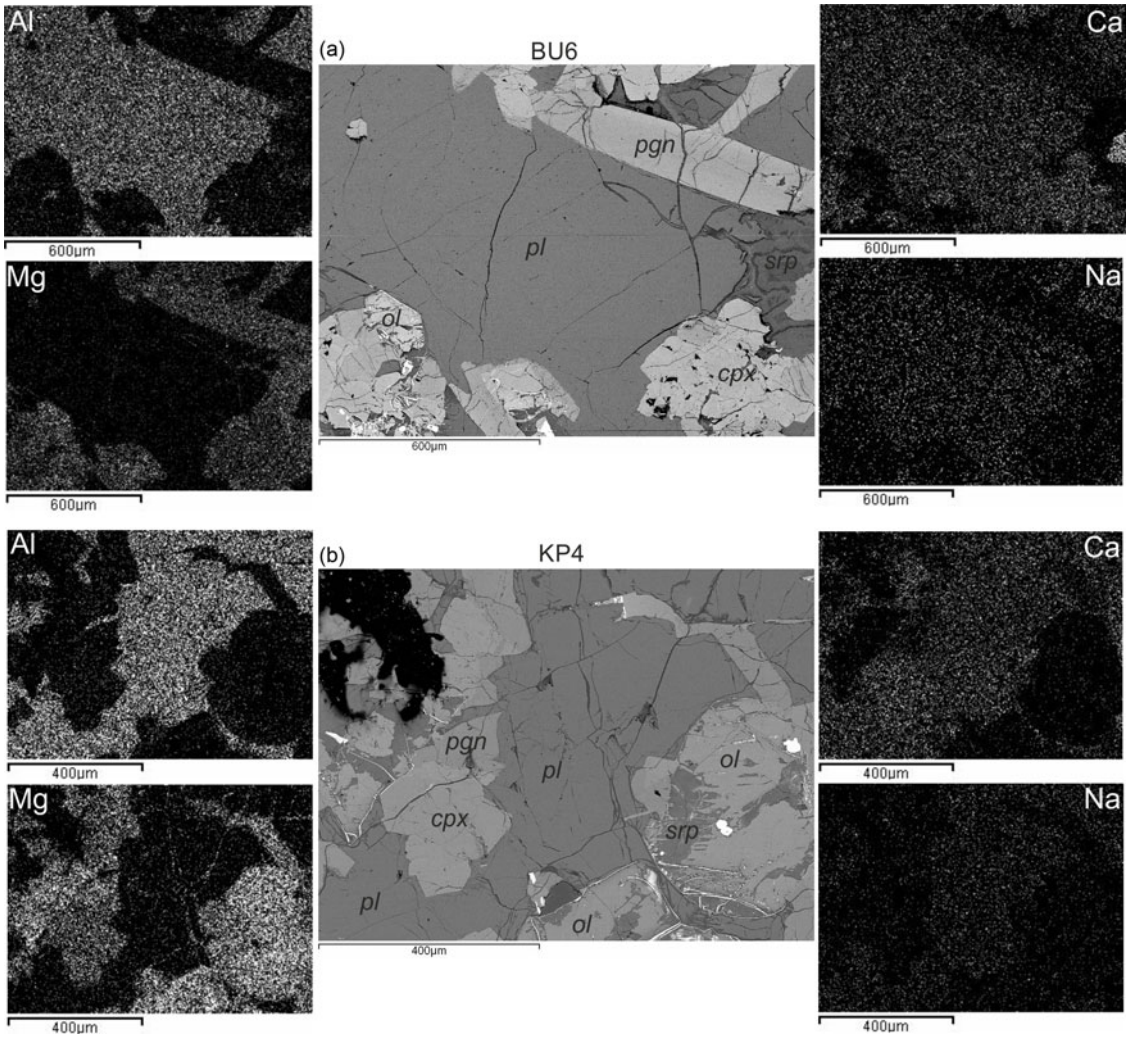

Figure 7. Back-scattered electron images (a, b) showing textural and compositional features of Khopoli olivine gabbros. The elemental maps (Al, Mg, Ca and Na) show limited chemical zonation in olivine, pyroxene and plagioclase crystals. Abbreviations: ol, olivine; pl, plagioclase; cpx, clinopyroxene; pgn, pigeonite; srp, serpentine.

4. d. True density

Cucciniello *et al.* (2014) measured a small range of true density values (3.02 to 3.06 g/cm^3) on samples of the Khopoli gabbro intrusion, whereas we measured a larger range of values, from 2.93 to 3.13 g/cm^3 (Supplementary Table S5). These density values are much higher than those typical of non-vesicular basalt (~2.8 g/cm^3, Best, 2003), and we explain their significance below.

5. Discussion

5. a. Geological and petrogenetic significance of the Khopoli intrusion

The ^{40}Ar/^{39}Ar age of the Khopoli intrusion obtained in this study shows that it formed contemporaneously with the Western Ghats tholeiitic lava sequence, which is dated at 66.5–65.5 Ma by ^{40}Ar/^{39}Ar and zircon U-Pb methods (Baksi, 2014; Renne *et al.* 2015; Schoene *et al.* 2015). The intrusion was emplaced at a shallow depth level, as suggested by its position within the volcanic sequence, and the low Al_2O_3 content of the augites (Cucciniello *et al.* 2014). Pressure values obtained with the barometer of Nimis (1999), based on clinopyroxene compositions only, range from 0.2 to 2.9 (± 1.8) kbar and indicate clinopyroxene crystallization during magma ascent or storage in the shallow crust (Melluso & Sethna, 2011; Cucciniello *et al.* 2014).

Accurate geological mapping of the intrusion (Mulay & Peshwa, 1980 and the present study, Fig. 3) shows that it does not fit any of the standard intrusion shapes. Godbole & Ray (1996) referred to it as the Khopoli picrite sill, but we can rule out topographic effects creating such a dyke-like outcrop of a horizontal sill. At the same time, the intrusion (which forms three aligned segments separated by basaltic lava flows) does not resemble a typical *en echelon* dyke. The Khopoli intrusion may have been a relatively broad, discontinuous and irregularly shaped feeder conduit of one of the many high-MgO lava flows of the Neral and Thakurvadi formations, which are known to contain considerable cumulus olivine and clinopyroxene (Beane, 1988; Beane and Hooper, 1988). The significant olivine-clinopyroxene cumulus enrichment within the Khopoli intrusion would then be as expected.

High-MgO rocks in the Deccan Traps only rarely represent primitive picritic liquids (e.g., Krishnamurthy & Cox, 1977; Krishnamurthy *et al.* 2000). Most Deccan high-MgO picritic rocks formed from basaltic liquids that accumulated olivine and

https://doi.org/10.1017/S0016756824000293 Published online by Cambridge University Press

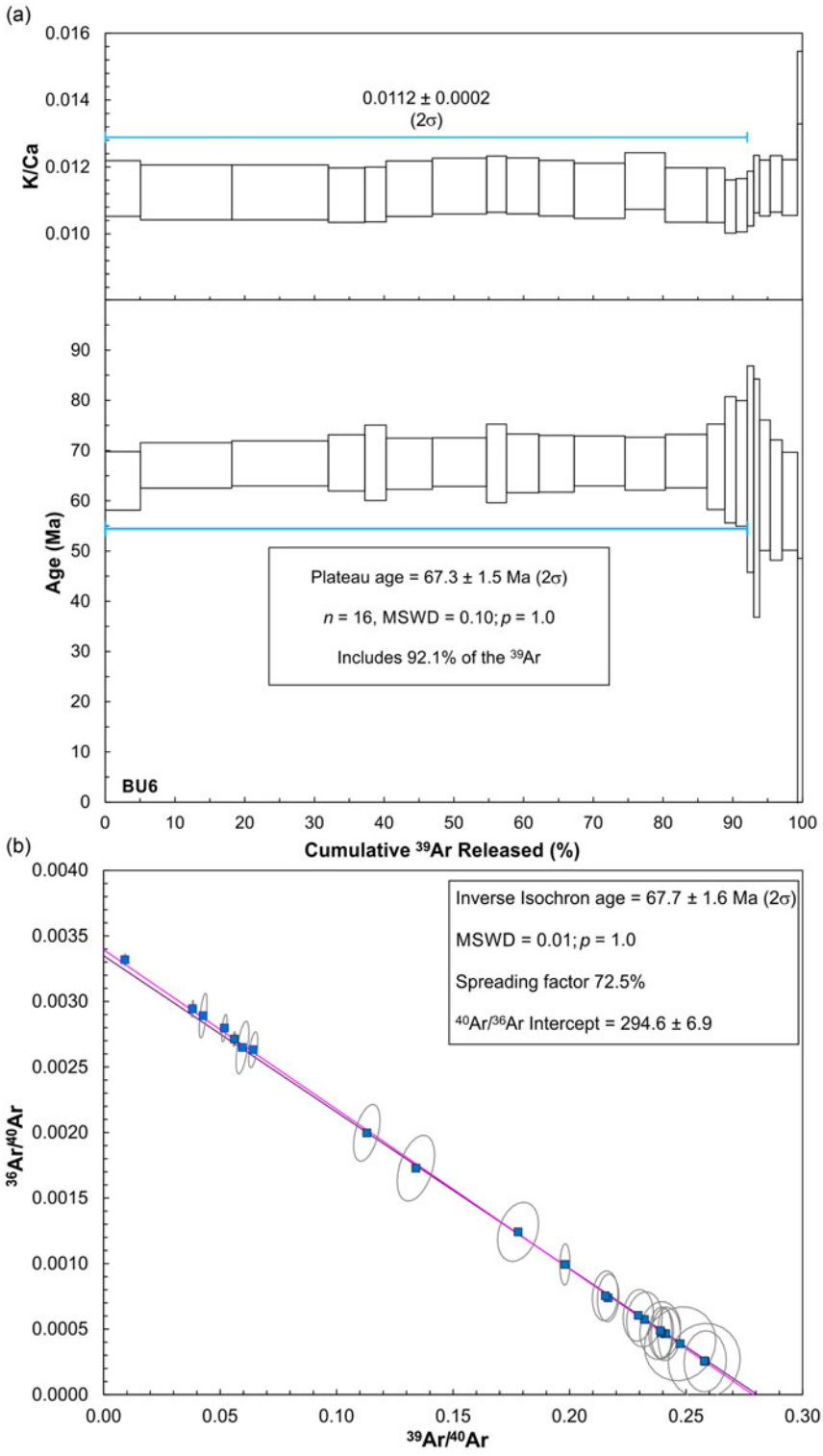

Figure 8. K/Ca plot and $^{40}Ar/^{39}Ar$ plateau age spectrum (a) and inverse isochron plot (b) for intercumulus plagioclase separates from the Khopoli olivine gabbro BU6. The blue horizontal line in (a) indicates the steps used in the plateau age calculation. The error on the plateau age is quoted at 2σ and includes all sources of uncertainty. MSWD and P values are indicated.

clinopyroxene. This is inferred from the relatively evolved olivine and clinopyroxene compositions not in equilibrium with bulk-rock Mg Number values (see e.g., Dongre *et al.* 2018). Beane & Hooper (1988) calculated that the maximum MgO contents of the Western Ghats basaltic liquids were 9–10 wt.% (see also Sen, 1988; Sethna & Sethna, 1988). Picrite and picritic basalt lava flows with cumulus olivine and clinopyroxene are common in the Neral and Thakurvadi Formations (Beane *et al.* 1986). For example, Thakurvadi picrite basalts KOP004 and KOP005, exposed in the Bor Ghat section at elevations of 127 m and 141 m, respectively, contain 13.2–14.2 wt.% MgO (Beane, 1988, p. 454), and MgO reaches 15.4 wt.% in other Thakurvadi lava flows (Khadri *et al.* 1988). Such rocks may represent mixtures between evolved tholeiitic basalt melts and the olivine-clinopyroxene crystal cargo left by earlier basaltic magmas in a chamber or conduit. However, some outcrops show clear field evidence of olivines and

https://doi.org/10.1017/S0016756824000293 Published online by Cambridge University Press

clinopyroxenes settling to the basal parts of lava flows under gravity and rendering the bases picritic (Beane & Hooper, 1988). A lava flow of the Neral Chemical Type (sample JEB251), exposed at 150 m elevation in the Bhivpuri section, has MgO as high as 24.83 wt.%, yet its most Mg-rich olivines only reach Fo_{79} (Beane, 1988, p. 64). Olivine gabbros of the Khopoli intrusion reach even greater MgO contents (~27 wt.%), yet their olivines are only $Fo_{78\text{-}71}$ in composition. These Deccan lava flows and intrusions constitute examples of substantial cumulus enrichment of olivine (and pyroxene).

5. b. Geophysical significance of the Khopoli intrusion

The Deccan Traps CFB province has been of considerable interest to geophysicists, who have reported large positive gravity and magnetic anomalies in various parts of the province, including the Mumbai area (e.g., Glennie, 1951; Takin, 1966). Modelling of these anomalies, carried out using plausible values of mantle and crustal rocks, has led to suggestions of yet-unexposed intrusions, crustal magma chambers, Moho upwarps, or mantle upwellings (e.g., Singh, 1998; Chandrasekhar *et al.* 2002; Bhattacharji *et al.* 2004). Other modelling (such as inversion of gravity and aeromagnetic data) has been used to provide estimates of unexposed basalt thicknesses and clues to ongoing seismicity (e.g., Nayak *et al.* 2006). Few geophysical studies, however, have used density values actually measured on samples of the Deccan basalts. These include Parthasarathy and Shah (1981), who measured densities of 2.78–3.01 g/cm^3 on massive (non-vesicular) Deccan basalts and 2.47–2.85 g/cm^3 on amygdaloidal basalts. Prasanna Lakshmi *et al.* (2014) measured densities of 2.42–3.00 g/cm^3 on vesicular and non-vesicular Deccan basalts from various stratigraphic formations, noting that basalt densities were systematically lower with increasing vesicularity and degree of weathering. Based on these studies, we use density values of 2.80–2.85 g/cm^3 as good estimates for non-vesicular, little-weathered Deccan basalt. There are no such density measurements on Deccan gabbroic rocks to our knowledge, with the exception of those by Cucciniello *et al.* (2014) on the Khopoli olivine gabbros. Whereas they measured true density values of 3.02–3.06 gm/cm^3, we have measured a larger range of true density values (2.93–3.13 g/cm^3, Supplementary Table S5). We also note that the least altered sample (KP22/01 with LOI 0.78 wt.%, Table 2) has the highest true density value.

This makes the Khopoli intrusion a feature of considerable geophysical interest. Thus, the large density difference between the Khopoli olivine gabbro intrusion (with measured true density values as high as 3.13 and no lower than 2.93 gm/cm^3) and its host basalt sequence (average density 2.80–2.85 g/cm^3 and much lower when vesicular and weathered) is expected to result in a significant positive gravity anomaly, when corrected for other factors such as topographic effects. We suggest therefore that not all high gravity anomalies known in the Deccan Traps may be deep-seated (crustal magma chambers or Moho upwarps); instead, high-density basic and ultrabasic intrusions such as the Khopoli olivine gabbro intrusion, emplaced at shallow depths within the Deccan volcanic pile, may be responsible for at least some of the anomalies observed.

6. Conclusions

The Khopoli olivine gabbro intrusion, emplaced within the Deccan flood basalts, is one of many intrusions exposed in the Konkan Plain, at the base of the Western Ghats escarpment. With bulk-rock MgO contents as high as 27 wt.% (on an anhydrous basis), it is one of the most magnesian Deccan rocks known, and its textural features and mineral compositions indicate that the olivine gabbros are olivine-pyroxene cumulates (Godbole & Ray, 1996; Cucciniello *et al.* 2014). We have dated the emplacement and crystallization of the Khopoli intrusion at 67.3 ± 1.5 Ma (2σ) using the $^{40}Ar/^{39}Ar$ technique on intercumulus plagioclase separates from one of the olivine gabbros. This age is consistent with the age of the Western Ghats CFB sequence. The Neral and Thakurvadi formations, into which the Khopoli intrusion has been emplaced, contain many lava flows enriched in cumulus olivine and clinopyroxene. The Khopoli intrusion may represent a relatively broad, discontinuous, irregularly shaped feeder conduit of one of these flows. Measured true density values of 2.93 to 3.13 g/cm^3 on the olivine gabbros of the Khopoli intrusion (Cucciniello *et al.* 2014 and the present study) suggest that such shallow-level mafic intrusions within the flood basalt pile may be the cause of many of the observed high gravity anomalies.

Supplementary material. The supplementary material for this article can be found at https://doi.org/10.1017/S0016756824000293

Acknowledgements. Leone Melluso and Sam Sethna are thanked for providing the sample BU6. We are grateful to Prof. Prabhakar Naraga for kindly permitting use of the XRF spectrometry facility (SIP Project; WBS Code: IN/22-1111039E-01) in the Department of Earth Sciences, IIT Bombay, and to Prof. Naraga and Dr. Trupti Chandrasekhar for personally supervising the analyses. We thank Andrea Marzoli and Igor Villa for helpful reviews of an earlier version of this manuscript. The present manuscript was considerably improved by the journal reviews of Renaud Merle and an anonymous referee, and the editorial handling of Sarah Sherlock.

Financial support. Fieldwork was supported by the research award project RI/0220-10000618-001 to Sheth from the Industrial Research and Consultancy Centre (IRCC), IIT Bombay. Funds for the $^{40}Ar/^{39}Ar$ analyses and elemental X-ray maps were provided by MIUR 2017 (grant 20178LPCPW_004 to C. Cucciniello). Shekhar and Astha were initially supported by Ph.D. Fellowships from IIT Bombay and are currently supported by the Prime Minister's Research Fellowship (PMRF, file numbers 1303100 and 1303103, respectively). Naik was supported by an IIT Bombay Institute Post-Doctoral Fellowship (File No. HR-1 (HRM-1)/Rect/33/2022/20003002).

References

Baksi AK (2014) The Deccan Trap – Cretaceous-Palaeogene boundary connection; new $^{40}Ar/^{39}Ar$ ages and critical assessment of existing argon data pertinent to this hypothesis. *Journal of Asian Earth Sciences* **84**, 9–23.

Beane JE (1988) Flow stratigraphy, chemical variation and petrogenesis of Deccan flood basalts from the Western Ghats, India. Ph.D. Dissertation, Washington State University, USA.

Beane JE and Hooper PR (1988) A note on the picrite basalts of the Western Ghats, Deccan Traps, India. In *Deccan Flood Basalts* (ed KV Subbarao), pp. 117–33. Bengaluru: Geological Society of India Memoir 10.

Beane JE, Turner CA, Hooper PR, Subbarao KV and Walsh JN (1986) Stratigraphy, composition and form of the Deccan basalts, Western Ghats, India. *Bulletin of Volcanology* **48**, 61–83.

Best MG (2003) *Igneous and Metamorphic Petrology*. 2nd ed. Blackwell Science Ltd.

Bhattacharji S, Sharma R and Chatterjee N (2004) Two- and three-dimensional gravity modelling along western continental margin and intraplate Narmada-Tapti rifts: its relevance to Deccan flood basalt volcanism. In *Magmatism in India through Time* (eds HC Sheth and K Pande). *Proceedings of the Indian Academy of Sciences (Earth & Planetary Sciences)* **113**, 771–784.

Chandrasekhar DV, Mishra DC, Poornachandra Rao GVS and Mallikharjuna Rao (2002) Gravity and magnetic signatures of volcanic

plugs related to Deccan volcanism in Saurashtra, India and their physical and geochemical properties. *Earth and Planetary Science Letters* **201**, 277–92.

Cucciniello C, Choudhary AK, Zanetti A, Sheth H, Vichare S and Pereira R (2014) Mineralogy, geochemistry and petrogenesis of the Khopoli mafic intrusion, Deccan Traps, India. *Mineralogy and Petrology* **108**, 333–51.

Cucciniello C, Sheth H, Duraiswami RA, Wegner W, Koeberl C, Das T and Ghule V (2020) The Southeastern Saurashtra dyke swarm, Deccan Traps: magmatic evolution of a tholeiitic basalt-basaltic andesite-andesite-rhyolite suite. *Lithos* **376–377**, 105759. doi: 10.1016/j.lithos.2020.105759.

Cucciniello C, Grifa C, le Roex AP, de' Gennaro R, Morra V and Melluso L (2023) Feeding system and mantle sources of the southern and western sector of the Madagascar flood basalt province, and comparisons with Southwest Indian Ridge "anomalous" basalts. *Lithos* **458-459**, 107361. doi: 10.1016/j.lithos.2023.107361.

Deshmukh SS and Sehgal MN (1988) Mafic dyke swarms in the Deccan volcanic province of Madhya Pradesh and Maharashtra. In *Deccan Flood Basalts* (ed KV Subbarao), pp. 323–40. Bengaluru: Geological Society of India Memoir 10.

Dessai AG and Viegas A (2010) Petrogenesis of alkaline rocks from Murud-Janjira, in the Deccan Traps, western India. *Mineralogy and Petrology* **98**, 297–311.

Dongre A, Viljoen KS and Rathod A (2018) Mineralogy and geochemistry of picro-dolerite dykes from the central Deccan Traps flood basaltic province, India, and their geodynamic significance. *Mineralogy and Petrology* **112**, 267–77.

Flanagan FJ (1984) Three USGS mafic rock reference samples, W-2, DNC-1, and BIR-1. *U.S. Geological Survey Bulletin* **1623**, 54 p.

Glennie EA (1951) Density or geological corrections to gravity anomalies for the Deccan Trap areas in India. *Geophysical Journal International* **6**, 179–93.

Godbole SM and Ray B (1996) Intrusive rocks of coastal Maharashtra. In *Deccan Basalts* (eds SS Deshmukh, KKK Nair, DB Yedekar, DM Mohabey and AK Chatterjee), pp. 233–50. Nagpur: Gondwana Geological Magazine Special Volume 2.

Jiang Q, Jourdan F, Olierook HKH, Merle RE, Verati C and Mayers C (2021) $^{40}Ar/^{39}Ar$ dating of basaltic rocks and the pitfalls of plagioclase alteration. *Geochimica et Cosmochimica Acta* **314**, 334–57.

Karmarkar BM (1978) The Deccan Trap basalt flows of the Bor Ghat section of Central Railway. *Journal of Geological Society of India* **19**, 106–14.

Khadri SFR, Subbarao KV, Hooper PR and Walsh JN (1988) Stratigraphy of Thakurvadi Formation, western Deccan basalt province, India. In *Deccan Flood Basalts* (ed KV Subbarao), pp. 281–304. Bengaluru: Geological Society of India Memoir 10.

Koppers AAP (2002) ArArCALC – software for $^{40}Ar/^{39}Ar$ age calculations. *Computers and Geosciences* **28**, 605–19.

Krishnamurthy P and Cox KG (1977) Picrite basalts and related lavas from the Deccan Traps of western India. *Contributions to Mineralogy and Petrology* **62**, 53–75.

Krishnamurthy P, Gopalan K and Macdougall JD (2000) Olivine compositions in picrite basalts and the Deccan volcanic cycle. *Journal of Petrology* **41**, 1057–69.

Kuehn SC, Froese DG, Shane PA and Participants II (2011) The INTAV intercomparison of electron-beam microanalysis of glass by tephrochronology laboratories: results and recommendations. *Quaternary International* **246**, 19–47.

Lee J-Y, Marti K, Severinghaus JP, Kawamura K, Yoo HS, Lee JB and Kim JS (2016) A redetermination of the isotopic abundances of atmospheric Ar. *Geochimica et Cosmochimica Acta* **70**, 4507–12.

Melluso L and Sethna SF (2011) Mineral compositions in the Deccan igneous rocks of India: an overview. In *Topics in Igneous Petrology* (eds J Ray, G Sen and B Ghosh), 135–60. Heidelberg: Springer.

Melluso L, Sethna SF, D'Antonio M, Javeri P and Bennio L (2002) Geochemistry and petrogenesis of sodic and potassic mafic alkaline rocks in the Deccan volcanic province, Mumbai area (India). *Mineralogy and Petrology* **74**, 323–42.

Melluso L, de'Gennaro R and Rocco I (2010) Compositional variations of chromiferous spinel in Mg-rich rocks of the Deccan Traps, India. *Journal of Earth System Science* **119**, 343–63.

Merle RE, Jiang Q, Jourdan F and Olierook H (2022) The age and origin of the Balleny and Scott volcanic provinces, Ross Sea, Antarctica. *Geochemistry* **82**, 125904. doi: 10.1016/j.chemer.2022.125904.

Middlemost AEK (1989) Iron oxidation ratios, norms and the classification of volcanic rocks. *Chemical Geology* **77**, 19–26.

Mishra KK (1971) Petrology of the picrite-basalt flows in the Igatpuri area, Nasik District, Maharashtra. *Bulletin of Volcanology* **35**, 957–64.

Mulay JG, Peshwa VV (1980) The occurrence of gabbroic intrusion in Deccan Trap basalts near Khopoli in the Konkan area (Maharashtra). *Current Science* **49**, 356–57.

Naik A, Sheikh JM, Sheth H, Samant H and D'Souza S (2021) Diverse late-stage (≤ 62.5 Ma) Deccan volcanism and plutonism in the Thane-Vasai region, Panvel flexure zone, western Indian rifted margin. *Journal of Earth System Science* **130**, 152. doi: 10.1007/s12040-021-01654-7.

Nayak GK, Agrawal PK, Rama Rao Ch and Pandey OP (2006) Thickness estimation of Deccan flood basalt of the Koyna area, Maharashtra (India) from inversion of aeromagnetic and gravity data and implications for recurring seismic activity. *Current Science* **91**, 960–65.

Nimis P (1999) Clinopyroxene geobarometry of magmatic rocks. Part 2. Structural geobarometers for basic to acid, tholeiitic and mildly alkaline magmatic systems. *Contributions to Mineralogy and Petrology* **135**, 62–74.

Ollier CD (1984) *Weathering*. 2nd ed. Longman, London, 304 p.

Parthasarathy, A and Shah SD (1981) Deccan volcanic-rock material and rock mass characteristics and their significance in engineering geology. In *Deccan Volcanism and Related Basalt Provinces in Other Parts of the World* (eds KV Subbarao and RN Sukheswala), pp. 233–43. Bengaluru: Geological Society of India Memoir 3.

Peng ZX, Mahoney J, Hooper P, Harris C and Beane J (1994) A role for lower continental crust in flood basalt genesis? Isotopic and incompatible element study of the lower six formations of the western Deccan Traps. *Geochimica et Cosmochimica Acta* **58**, 267–88.

Phillips D and Matchan EL (2013) Ultra-high precision $^{40}Ar/^{39}Ar$ ages for Fish Canyon tuff and alder creek rhyolite sanidine: new dating standards required? *Geochimica et Cosmochimica Acta* **121**, 229–39.

Powar KB and Vadetwar SV (1995) Mineralogy and geochemistry of basic dykes and associated plugs of the Revas-Murud sector, Konkan coastal belt, Maharashtra. In *Dyke Swarms of Peninsular India* (ed TC Devaraju), pp. 339–63. Bengaluru: Geological Society of India Memoir 33.

Prasanna Lakshmi KJ, Senthil Kumar P, Ravinder S, Seshunarayana T and Sen MK (2014) Petrophysical properties of the Deccan basalts exposed in the Western Ghats escarpment around Mahabaleshwar and Koyna, India. In Flood Basalts of Asia (eds H Sheth and L Vanderkluysen). Journal of Asian Earth Sciences **84**, 176–87.

Renne PR, Mundil R, Balco G, Min K and Ludwig KR (2010) Joint determination of ^{40}K decay constants and $^{40}Ar^*/^{40}K$ for the Fish Canyon sanidine standard, and improved accuracy for $^{40}Ar/^{39}Ar$ geochronology. *Geochimica et Cosmochimica Acta* **74**, 5349–67.

Renne PR, Balco G, Ludwig KR, Mundil R, Min K (2011) Response to the comment by W.H. Schwarz *et al.* on "Joint determination of 40K decay constants and 40Ar*/40K for the Fish Canyon sanidine standard, and improved accuracy for 40Ar/39Ar geochronology" by P.R. Renne *et al.* (2010). *Geochimica et Cosmochimica Acta* **75**, 5097–100.

Renne PR, Deino AL, Hilgen FJ, Kuiper KF, Mark DF, Mitchell III WS, Morgan LE, Mundil R and Smit J (2013) Time scales of critical events around the Cretaceous-Palaeogene boundary. *Science* **339**, 684–87.

Renne PR, Sprain CJ, Richards MA, Self S, Vanderkluysen L and Pande K (2015) State shift in Deccan volcanism at the Cretaceous-Palaeogene boundary, possibly induced by impact. *Science* **350**, 76–78.

Schoene B, Samperton KM, Eddy MP, Keller G, Adatte G, Bowring SA, Khadri SFR and Gertsch B (2015) U-Pb geochronology of the Deccan Traps and relation to the end-Cretaceous mass extinction. *Science* **347**, 182–84.

Sen G (1988) Possible depth of origin of primary Deccan tholeiite magma. In *Deccan Flood Basalts* (ed KV Subbarao), pp. 35–51. Bengaluru: Geological Society of India Memoir 10.

Sethna SF and Sethna BS (1988) Mineralogy and petrogenesis of Deccan Trap basalts from Mahabaleshwar, Igatpuri, Sagar and Nagpur areas, India. In *Deccan Flood Basalts* (ed KV Subbarao), pp. 69–90. Bengaluru: Geological Society of India Memoir 10.

Sethna SF and Sethna BS (1990) Petrology of Deccan Trap basalts of the Western Ghats around Igatpuri and their petrogenetic significance. *Journal of Geological Society of India* **35**, 631–43.

Sheth H (2018) *A Photographic Atlas of Flood Basalt Volcanism*. Springer, New York, 363 p.

Singh AP (1998) 3-D structure and geodynamic evolution of accreted igneous layer in the Narmada–Tapti region (India). *Journal of Geodynamics* **25**, 129–41.

Subbarao KV and Hooper PR (1988) Reconnaissance map of the Deccan Basalt Group in the Western Ghats, India. In *Deccan Flood Basalts* (ed KV Subbarao), enclosure. Bengaluru: Geological Society of India Memoir 10.

Sukheswala RN and Sethna SF (1962) Deccan Traps and associated rooks of Basssin area. *Journal of Geological Society of India* **3**, 125–46.

Takin M (1966) An interpretation of the positive gravity anomaly over Bombay on the west coast of India. *Geophysical Journal International* **11**, 527–37.

Van Keulen J (1973) Density of porous solids. *Materials and Structures* **6**, 181–83.

Verma SP, Torres-Alvarado IS and Sotelo-Rodriguez ZT (2002) SINCLAS: standard igneous norm and volcanic rock classification system. *Computers and Geosciences* **28**, 711–15.

Yatheesh V (2020) Structure and tectonics of the continental margins of India and the adjacent deep ocean basins: current status of knowledge and some unresolved problems. *Episodes* **43**, 586–608.

https://doi.org/10.1017/S0016756824000293 Published online by Cambridge University Press